Spanwise gradients in flow speed help stabilize leading-edge vortices on revolving wings

T. Jardin[1] and L. David[2]

[1]*Institut Supérieur de l'Aéronautique et de l'Espace, University of Toulouse, 10 avenue Edouard-Belin, Toulouse, 31055, France*

[2]*Institut Pprime, University of Poitiers, 11 boulevard Marie et Pierre Curie, Futuroscope Chasseneuil, 86962, France*

While a leading edge vortex on an infinite translating wing is shed after a short distance of travel, its counterpart on a finite span revolving insect wing or maple seed membrane exhibits robust attachment. The latter explains the aerodynamic lift generated by such biological species. Here we analyze the mechanisms responsible for leading edge vortex attachment. We compute the Navier-Stokes solution of the flow past a finite span wing (1) embedded in a uniform oncoming flow, (2) embedded in a spanwise varying oncoming flow and (3) revolving about its root. We show that over flapping amplitudes typical of insect flight ($\phi = 120°$) the spanwise gradient of the local wing speed may suffice in maintaining leading edge vortex attachment. We correlate this result with the development of spanwise flow, driven by the spanwise gradient of pressure, and we evaluate the sensitivity of such a mechanism to the Reynolds number. It is noted, however, that leading edge vortex attachment through the spanwise gradient of the local wing speed does not promote large lift, which ultimately arises from centrifugal and Coriolis effects.

INTRODUCTION

In 1996, Ellington *et al.* [1] reported major advances in the understanding of insect flight, exploding the myth that 'bees cannot fly' [2]. By visualizing the flow around a revolving wing, the research team from Cambridge University has brought to the fore the existence of an intense leading-edge vortex closely attached to the wing's surface. It is now widely accepted that such a vortex is a principal contributor to the aerodynamic lift generated by an insect wing [3, 4]. Prior to this breakthrough, conventional aerodynamic theories failed to predict the lift generated by a hovering insect.

A comparable approach by Lentink *et al.* [5] elegantly revealed the existence of a very similar coherent vortical structure, this time at the surface of a falling maple seed membrane. This observation shed light on the dispersal mechanism of such plant species which may be carried by the wind over large distances away from the parent plant, potentially enhancing seedling survival. Evidence was presented showing that 'maple seeds and insects exploit the same trick to fly'.

Although fascinating in themselves, these findings raise an underlying question: what causes the Leading Edge Vortex (LEV) to remain attached to the wing/seed membrane's surface while its counterpart on a pseudo-infinite translating wing (at a similar Reynolds number and angle of attack) sheds into the wake, resulting in a drastic drop in the aerodynamic lift ? The answer to this question is not trivial and the problem could be restated in a simpler fashion: what are the differences between a revolving insect wing/seed membrane and a pseudo-infinite translating wing ? The logical answer comes in three parts: (1) the relative contribution of the tip vortex to the global flow dynamics (associated with the wing's aspect ratio); (2) the spanwise gradient of the local wing speed (imposed by the revolving motion); and (3) centrifugal and Coriolis effects, referred to as fictitious effects (inherent to the revolving motion).

Recent numerical and experimental studies have addressed the first issue [6–8]. Overall, it has been suggested that the tip vortex on a translating wing may play a role in the attachment of the LEV over a finite portion of the wing, in the vicinity of the wing tip. This portion of the wing appears to be independent of the wing aspect ratio and is limited to approximately 1.5 times the wing chord. This observation excludes the idea that the tip vortex might be responsible for the LEV attachment on wings with a semi-span exceeding 1.5 times the wing chord, as used by dragonflies, for example.

More extensive research has simultaneously addressed the second and third issues (*i.e.* coupled issues)[9–11]. Following the analogy with the LEV of delta wings, it has been suggested that a spanwise flow balances vorticity production at the leading edge of a revolving wing, preventing vorticity accumulation inside the LEV and hence avoiding vortex shedding. Although it is expected that such spanwise flow arises from both fictitious effects (centrifugal) and the spanwise gradient of the local wing speed, there is no evidence that either one is more crucial in sustaining LEV attachment. This lack of evidence comes from the difficulty in dissociating these mechanisms experimentally, both being intrinsic to revolving motion. In contrast, numerical approaches offer an in-

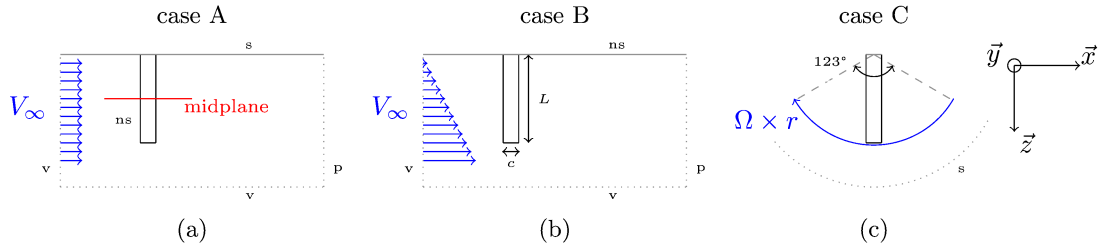

FIG. 1: (Color online) Top view of the three configurations (A,B,C) used for the simulations. (a) The finite wing is embedded in a uniform oncoming flow. This case models a translating wing for which the local speed along the semi-span L is constant. (b) The wing is subjected to a spanwise varying oncoming flow. The spanwise variation of the flow velocity is linear and models the variation of local wing speed imposed by a revolving motion. The spanwise variation is fixed so as to ensure identical local wing speed (hence identical local Reynolds number) for cases A, B and C at the wing midplane. (c) The wing revolves about its root. The local wing speed is similar to that in case B, *i.e.* $\Omega \times r = V_\infty$ where Ω is the revolving speed and r is the local wing radius. However the case differs due to the influence of fictitious effects. Symbols v, p, s and ns stand for velocity, pressure, slip and no-slip boundary conditions. The computational domain is shown for illustration purposes; upstream and side boundaries are actually located $10c$ away from the wing while downstream boundaries are located $30c$ away from it.

teresting opportunity to tackle the problem and build a comprehensive picture of leading edge vortex attachment on revolving wings.

Thus, the goal of this work is to isolate the mechanisms associated with the spanwise gradient of the local wing speed from the mechanisms associated with fictitious forces, and to evaluate their interplay with LEV development. Toward that end, we compute the Navier-Stokes solution of the flow around a finite wing (1) subjected to a uniform oncoming flow, (2) subjected to a spanwise varying oncoming flow and (3) revolving about its root. These configurations will henceforth be referred to as cases A, B and C, respectively (Fig. 1).

NUMERICAL SETUP

The wing profile is a 2.5% thickness flat plate with elliptic leading and trailing edges. The wing aspect ratio is set to $\mathcal{AR} = L/c = 4$, where L and c are the semi-span and chord length respectively. The wing angle of attack is fixed to $\alpha = 45°$, far beyond the stall limit of the profile. In all cases, the $\vec{z}$ axis is directed along the span towards the wing tip, the $\vec{y}$ axis is in the vertical direction and the $\vec{x}$ axis is in the horizontal direction, *i.e.* colinear to the wing speed. The Navier-Stokes equations are directly solved using a finite volume method. The grid consists of 5 million polyhedral cells, with a typical grid spacing in all three dimensions of $0.02c$ in the vicinity of the wing. The time step is fixed to meet the Courant-Friedrichs-Lewy condition. Second order schemes are used for both spatial and temporal discretizations. The results presented are converged with respect to computation parameters (grid size, time step, location of external boundary conditions) and non-dimensionalized with respect to the wing chord c and the mean wing speed along the span $\widetilde{V_\infty}$. Furthermore, the approach has proven its ability to accurately predict the flow past moving bodies [8] and, more generally, the occurence of flow instabilities at low Reynolds numbers [12, 13].

The total non-dimensional distance traveled by the wing is set to $\delta = 4.3$. In the case of a revolving wing (case C), this corresponds to a revolution amplitude $\phi = 123°$, typical of insect wings kinematics.

FLOW STRUCTURE

Figure 2 shows λ_2-criterion isosurfaces produced under the three different flow conditions at three distances of travel at a Reynolds number $\mathrm{Re} = c\widetilde{V_\infty}/\nu = 500$ (where ν is the kinematic viscosity of the surrounding fluid). λ_2 is the second eigenvalue of the symmetrical part of the incompressible Navier-Stokes equation gradient, neglecting unsteady and viscous terms, and is used to identify vortex cores [14]. In all cases, the flow is characterized by the development of a Starting Vortex (SV), a Tip Vortex (TV) and a Leading Edge Vortex (LEV). However, fundamental differences in the evolution of these structures are observed between case A and cases B and C. In case A, the LEV rapidly sheds into the wake, except in the vicinity of the wing tip where it experiences the influence of the TV. Conversely, in cases B and C, the LEV remains attached along most of the span, except in the vicinity of the wing tip where it sheds and merges with the TV. At $\delta = 4$ the latter bursts into a non-coherent structure. The extent of this non-coherent region is larger in case B than in case C, suggesting that fictitious effects mitigate laminar-to-turbulent transition.

Although it can be observed that cases B and C exhibit roughly similar flow structure and significantly differ from case A in that LEV attachment seems considerably promoted, a thorough comparison between the three cases remains ambiguous at this point. Indeed, δ being

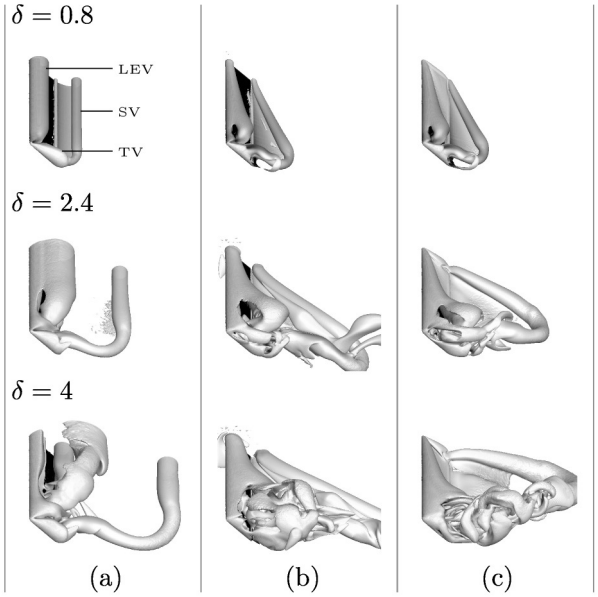

FIG. 2: Comparison of $\lambda_2 < 0$ criterion isosurfaces obtained for cases A (a), B (b) and C (c) at three distances of travel $\delta = 0.8$, $\delta = 2.4$ and $\delta = 4$ for Re $= 500$.

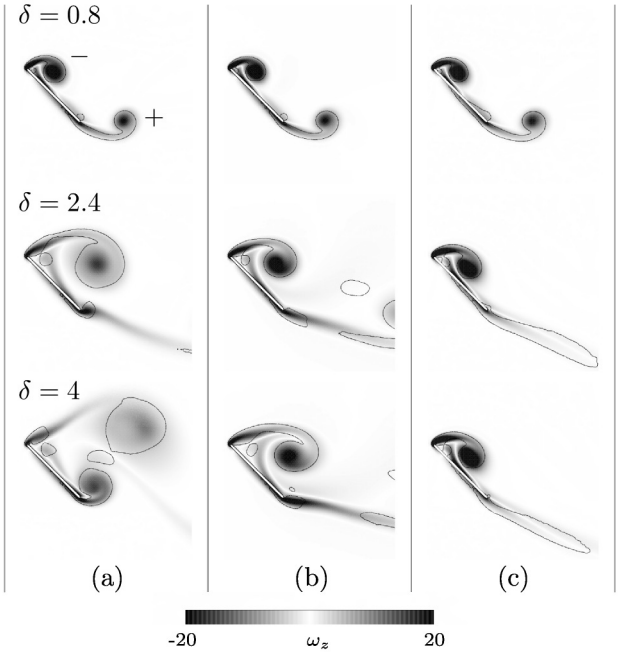

FIG. 3: Comparison of spanwise vorticity contours ω_z and $\lambda_2 < 0$ criterion isolines obtained for cases A (a), B (b) and C (c) at three distances of travel $\delta = 0.8$, $\delta = 2.4$ and $\delta = 4$ for Re $= 500$. LEV shedding is only observed in case A. $+$ and $-$ symbols indicate the sign of vorticity.

non-dimensionalized with respect to $\widetilde{V_\infty}$, which is equal to the local value of V_∞ at the midplane, it is expected that the LEV in cases B and C sheds at larger δ in the inner portion of the wing and at smaller δ in the outer portion of the wing when compared to case A. Therefore, in order to clarify this ambiguity, a local analysis is conducted in the next section.

LEADING-EDGE VORTEX

We focus on the dynamics of the leading edge vortex in the midplane of the wing. The non-dimensional distance traveled by the wing in the midplane is equivalent for all three cases. The local Reynolds number $\mathrm{Re} = cV_\infty/\nu$ at the midplane is also identical for all three cases and is equivalent to the global Reynolds number, since V_∞ at the midplane is equal to $\widetilde{V_\infty}$.

We first consider a Reynolds number Re $= 500$. Figure 3 shows the spanwise vorticity ω_z iso-contours produced in the midplane under the three different flow conditions at three distances of travel. λ_2 criterion isolines are also depicted as it allowed us to evaluate the circulation of the leading edge vortex $\Gamma = \int_\Sigma \omega_z dS$, where the vortex core Σ is defined as a region of negative λ_2, *i.e.* enclosed within a $\lambda_2 = 0$ isoline. The evolution of $|\Gamma|$ against δ is plotted in figure 4.

In case A, the LEV rapidly develops after the impulsive start of the wing. Its formation rate $\partial\Gamma/\partial\delta$ is rather

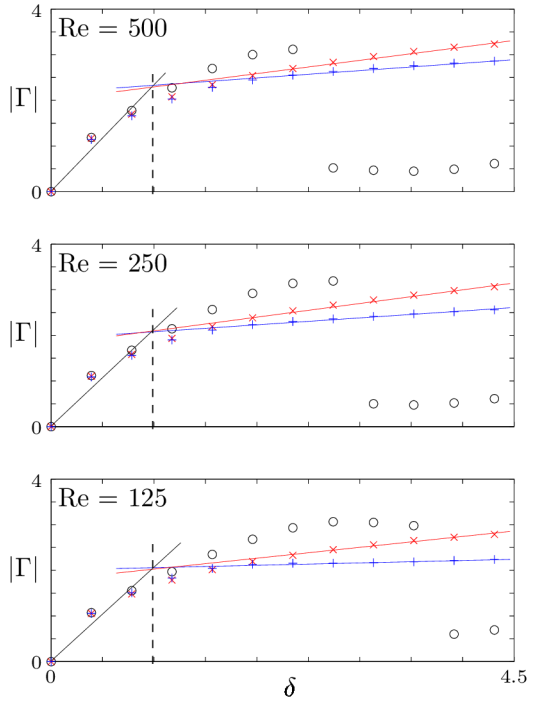

FIG. 4: (Color online) Circulation Γ of the LEV against distance δ traveled by the wing. Γ is obtained for cases A ($\circ$), B ($\times$) and C ($+$) by integrating the spanwise vorticity ω_z over the region Σ enclosed within a $\lambda_2 < 0$ isoline.

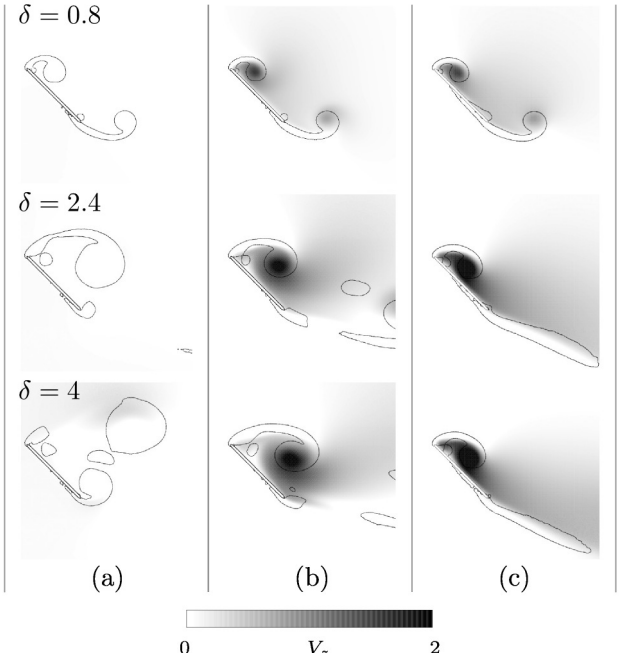

FIG. 5: Comparison of spanwise velocity contours V_z and $\lambda_2 < 0$ criterion isolines obtained for cases A (a), B (b) and C (c) at three distances of travel $\delta = 0.8$, $\delta = 2.4$ and $\delta = 4$ for Re = 500. Note that the colormap is cut at 0 such that negative velocities are displayed as white contours.

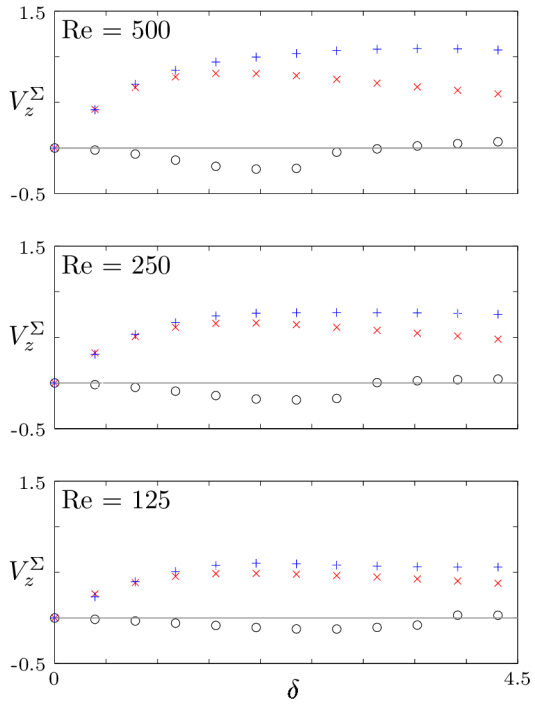

FIG. 6: (Color online) Mean spanwise velocity V_z^Σ of the LEV against distance δ traveled by the wing. V_z^Σ is obtained for cases A ($\circ$), B ($\times$) and C ($+$) by averaging the spanwise velocity V_z over the region Σ enclosed within a $\lambda_2 < 0$ isoline.

intense during the early stages of the wing motion. From $\delta = 0$ to $\delta = 2.4$, it can be observed that the LEV grows in size while the center of its core moves away from the wing. Eventually, the LEV sheds into the wake near $\delta = 2.5$ due to the combination of the vorticity accumulation and cross-wake interactions with the trailing edge vortex [15]. This is accompanied by a severe drop in its circulation as the vorticity contained in the leading edge shear layer no longer contributes to it.

In case B, the evolution of Γ follows a comparable trend to that observed in case A during the very early stages of the wing motion. It then diverges from the latter, around $\delta = 1$, to adopt a lower growth rate that tends to a constant value. Figure 3 indicates that this new trend is associated with the continuous attachment of the LEV. Here, the spanwise gradient of the local wing speed induces a spanwise gradient of pressure along the wing span, and a spanwise variation of the LEV strength. Hence a spanwise flow V_z develops, directed towards the wing tip, *i.e.* towards high velocity and low pressure regions, and mostly concentrated in the core of the vortex (Fig. 5). Though not shown here for the sake of conciseness, a spanwise gradient of pressure is clearly visible in our simulations, as was first speculated by Ellington *et al.* for revolving wings [1]. These mechanisms contribute to the spanwise advection of vorticity that balances the production of vorticity at the leading edge. The mean spanwise velocity in the core of the leading edge vortex V_z^Σ is plotted against δ in figure 6. It demonstrates that V_z^Σ reaches a maximum value of the order of 0.8 near $\delta = 2$ in case B while it is mostly negative (directed towards the root) in case A. As such, we provide a first piece of evidence that the spanwise gradient of the local wing speed alone, *via* vorticity advection, may suffice in maintaining LEV attachment on typical insect wings, *i.e.* with an amplitude of revolution around $\phi = 120°$.

In case C, the circulation growth rate is further mitigated (Fig. 4). In contrast with case B, the mean spanwise velocity of the LEV does not decrease after $\delta = 2$ but rather saturates at a value of the order of 1 (Fig. 6), hence maintaining the level of spanwise vorticity drainage out of the LEV core. The enhancement of V_z^Σ, with respect to the value obtained for case B, highlights the influence of fictitious forces. As a consequence, the vortex exhibits a compact shape (smaller core and higher vorticity levels) robustly attached to the wing's surface (Fig. 3).

We then investigate similar cases at Reynolds numbers Re = 250 and Re = 125. The evolution of $|\Gamma|$ against δ obtained for both Re is plotted in figure 4 to facilitate comparison with that obtained at Re = 500.

In case A, it is shown that the maximum circulation attained by the LEV is very similar for all three Reynolds numbers, of the order of $|\Gamma_{max}| = 3.1$. On the other hand, this maximum value, which thus appears as a vorticity accumulation threshold beyond which vortex at-

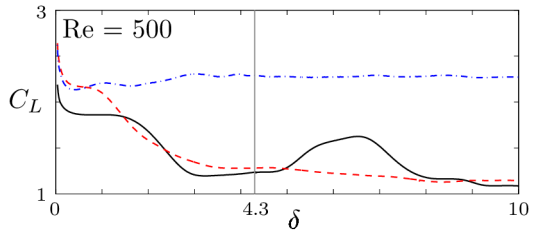

FIG. 7: (Color online) Lift coefficient C_L against distance δ traveled by the wing. C_L is obtained for cases A (plain), B (dashed) and C (dash-dotted) by non-dimensionalizing the lift force of the wing using the mean wing speed along the span $\widetilde{V_\infty}$.

tachment can no longer be maintained, is reached at larger δ values. This indicates that viscous effects mediate the LEV development and may suffice in maintaining LEV attachment over typical flapping amplitudes at even lower Reynolds numbers (or alternatively at moderate Reynolds numbers and lower flapping amplitudes).

The mitigation of LEV development with respect to viscous effects is also highlighted for cases B and C. Overall, it can be seen from figure 4 that $|\Gamma|$ decreases with Re at a given δ.

However, the relative trends of cases B and C circulation curves (as well as V_z^Σ curves in figure 6) are roughly similar for all Reynolds numbers. As such, the concomittance of viscous effects, the spanwise gradient of the local wing speed and fictitious effects in the specific case C at Re = 125 are found to almost completely damp the circulation growth rate. Here, the evolution of Γ against δ roughly reaches a steady-state that is likely to highlight LEV attachment over a very large distance of travel.

AERODYNAMIC LOADS

Finally, we ask if leading edge vortex attachment through spanwise gradient in flow speed has a beneficial effect on lift production. Figure 7 shows the lift coefficient C_L as a function of the non-dimensional distance traveled by the wing δ for cases A, B and C at Reynolds number Re = 500. Although the focus is on flapping amplitudes of the order of 120° (*i.e.* $\delta = 4.3$), results are shown for distances of travel up to $\delta = 10$. This constitutes a first step towards the extension of previous results to the analysis of spinning seeds with very large δ.

As expected, the lift produced by the translating wing (case A) rapidly drops as the LEV sheds into the wake. Furthermore, subsequent bump in C_L history near $\delta = 6.6$ indicates the onset of periodic build-up and shedding of leading and trailing edge vortices, along with the development of a von Karman vortex street.

A striking feature is the decrease of C_L in case B, where the LEV is found to remain attached to the wing throughout the whole stroke (*i.e.* up to $\delta = 4.3$). Figure 3 suggests that this trend in C_L is associated with the progressive increase of wing surface / LEV core distance. In addition, although this distance increases, C_L history makes no evidence of von Karman vortex street development after $\delta = 4.3$ (no subsequent peak), and up to $\delta = 10$. Rather, the flow structure remains roughly similar to that observed in figure 2 (case B, $\delta = 4$), the LEV being attached to the wing, yet with the extent of the bursted tip region towards the wing midplane.

Conversely, the robust attachment of the LEV close to the wing surface in case C maintains a large C_L throughout the whole stroke. What is more, the amount of lift produced by the rotating wing remains constant up to $\delta = 10$. Hence, it is shown that although spanwise gradient in flow speed helps stabilize the LEV, fictitious effects are the ultimate key factor in lift generation on revolving flapping wings.

CONCLUSION

The results outlined in this paper suggest that fictitious effects are not a requirement for leading edge vortex attachment on revolving insect wings, although they do contribute to it. In particular, it is shown that a spanwise gradient in flow speed may suffice in maintaining LEV attachment over typical flapping amplitudes, on the order of $\phi = 120°$. Viscous effects may also suffice, typically for Reynolds numbers below 100. Overall, the analysis indicates that viscosity, the spanwise gradient of the local wing speed and fictitious effects all contribute to LEV attachment such that, for Reynolds numbers of the order of 100, their concomitancy may ensure LEV attachment over very large distances of travel. However, leading edge vortex attachment through spanwise gradient in flow speed or viscous effects is not, on its own, responsible for large sustained lift on revolving wings. Rather, by anchoring the LEV even closer to the wing surface, fictitious effects appear to be the ultimate key factor in lift generation. Hence, LEV attachment is a necessary but not sufficient condition for high lift generation, which is ultimately ensured by a short wing surface / LEV core distance.

These findings contribute to the fundamental understanding of revolving wing aerodynamics and offer new perspectives in the development of micro-air vehicles. New perspectives notably include more accurate modeling of LEV development, and subsequent wake capture mechanisms that occur on flapping wings, which contributes to the definition of optimum flapping wing kinematics. Similar reasoning may also be applied in order to shed light on the vortex dynamics and forces experienced by bodies in shear flows, covering a wide range of applications, from hair flow sensors to atmospheric or seabed boundary layers installations [16, 17].

[1] C.P. Ellington, C. van den Berg, A.P. Willmott and A.L.R. Thomas, Nature **384**, 626 (1996).
[2] A. Magnan, La locomotion chez les animaux, Paris : Hermann et Cie (1934).
[3] M.H. Dickinson, F.O. Lehmann and S.P. Sane, Science **284**, 1954 (1999).
[4] Z.J. Wang, Annu. Rev. Fluid Mech. **37**, 183 (2005).
[5] D. Lentink,W.B. Dickson, J.L. van Leeuwen and M.H. Dickinson, Science **324**, 1438 (2009).
[6] M.J. Ringuette, M. Milano and M. Gharib, J. Fluid Mech. **581**, 453 (2007).
[7] K. Taira and T. Colonius, J. Fluid Mech. **623**, 187 (2009).
[8] T. Jardin, A. Farcy and L. David, J. Fluid Mech. **702**, 102 (2012).
[9] J.M. Birch, M.H. Dickinson, Nature **412**, 729 (2001).
[10] D. Lentink and M.H. Dickinson, J. Exp. Biol. **212**, 2705 (2009).
[11] C.M. Ozen and D. Rockwell, J. Fluid Mech. **707**, 541 (2012).
[12] T. Jardin and Y.Bury, J. Fluid Mech. **696**, 285 (2012).
[13] Y. Bury and T. Jardin, Phys. Letters A **376**, 3219 (2012).
[14] F. Hussain and J. Jeong, J. Fluid Mech. **285**, 69 (1995).
[15] C.H.K. Williamson, Annu. Rev. Fluid Mech. **28**, 477 (1996).
[16] Z. Fan, J. Chen, J. Zou, D. Bullen, C. Liu and F. Delcomyn, J. Micromech. Microeng. **12**, 655 (2002).
[17] O.M. Griffin, ASME Trans. J. Fluids Eng. **107**, 298 (1985).